Experimental Demonstration of Enhanced Hydrogen Permeation in Palladium Via a Composite Catalytic-Permselective Membrane

Daejin Kim, Kevin Barnett, and Benjamin A. Wilhite
Artie McFerrin Dept. of Chemical Engineering, Texas A&M University, College Station, TX 77843

DOI 10.1002/aic.13921
Published online September 28, 2012 in Wiley Online Library (wileyonlinelibrary.com).

A composite catalytic-permselective (CCP) membrane comprised of a 500-μm Cu(II)O/Al_2O_3 catalyst film washcoated overtop a 27-μm electroless-plated dense palladium thin film was constructed on a porous less-steel substrate. Hydrogen purification experiments performed under ideal (H_2–Ar) nonreactive mixtures and simulated reformate (5% CO, 7.5% H_2O, 15% H_2, 1.5% CO_2, and balance Ar) over a range of residence times at 623–773 K confirm up to 30% enhancement in observed hydrogen permeance of the palladium film, achieved using the CCP membrane design in which the catalyst layer modifies the gas-phase composition in direct contact with the permselective Pd film. Scanning electron microscopy analysis of the palladium film after ~10-h exposure to reaction conditions and Cu(II)O catalyst confirm no corrosion of the film, while observed hydrogen permselectivities remained in excess of 10,000:1. These experimental results confirm that the CCP membrane design is capable of significantly improving palladium membrane performance. © 2012 American Institute of Chemical Engineers *AIChE J,* 59: 1627–1634, 2013

Keywords: gas purification, membrane separations, composite membranes, fuels, energy

Introduction

There has been significant interest over the past two decades toward developing efficient hydrogen purification technologies in support of enhancing the sustainability and resource flexibility of our energy and fuels infrastructure.[1,2] Hydrogen is currently used in the catalytic upgrading of petroleum distillates to increase the yield of transportation and logistics fuels.[3] The growth of the biorefinery industry for producing alternative fuels from domestic and renewable resources is expected to increase hydrogen demand, as current biofuels require significant upgrading and reforming to achieve combustion properties comparable to petroleum distillates.[2] In addition to its use in hydrocarbon fuels production, hydrogen is a promising fuel in its own right, as it is derivable from virtually any hydrocarbon resource. Hydrogen-driven polymer-electrolyte membrane fuel cells (PEMFCs) promise significant improvement in system efficiencies, as compared to existing combustion-based power systems, thus, making hydrogen technology a promising means for achieving greater sustainability and resource flexibility.[4–6]

Currently, 95% of industrial hydrogen is produced from fossil resources including natural gas, coal, and petroleum distillates using pyrolysis and/or catalytic reforming,[1] whereas production of hydrogen from liquid logistical fuels such as methanol and diesels is performed primarily by catalytic reforming.[2] The resulting reformate gas contains carbonaceous impurities primarily consisting of CO, which significantly limits PEMFC performance at concentrations above 5 ppm.[2,4,7] Downstream incorporation of water–gas-shift reaction (Eq. 1) is typically used to boost hydrogen yields while reducing carbon monoxide concentration

$$\mathrm{CO} + \mathrm{H_2} \leftrightarrow \mathrm{CO_2} + \mathrm{H_2} \quad \Delta H_{298} = -41.1 \ \mathrm{kJ\ mol^{-1}} \qquad (1)$$

Further purification of hydrogen to below the 5 ppm CO threshold can be achieved using a dense-permselective palladium or palladium–alloy membrane. Palladium membranes exhibit infinite theoretical hydrogen permselectivities owing to a hydrogen-specific transport mechanism comprised of dissociative chemisorption of molecular hydrogen at the metal surface, followed by diffusion of atomic hydrogen through the dense metal film.[8] The resulting ultrahigh-purity hydrogen permeate meets the stringent CO restrictions of the PEM fuel cell.[8,9] The permeability of the palladium membrane can be significantly reduced upon exposure to reformate impurities such as ammonia,[10] carbon monoxide,[11–13] chlorine,[14,15] ethylene,[16] methane,[16,17] propylene,[17] and sulfur.[18,19] For the case of carbon monoxide contaminant, multiple authors have confirmed permeation losses up to 10–65% upon exposure to 10%, typical of diesel reformate mixtures.[11,12,20]

The challenge of palladium film corrosion and/or inhibition upon exposure to reformate chemistries can be met using a composite membrane design, wherein a porous catalytic layer is coupled with the dense palladium film (shown schematically in Figure 1). In this composite catalytic-permselective (CCP) membrane design, the catalyst layer provides

Correspondence concerning this article should be addressed to B. A. Wilhite at benjamin.wilhite@che.tamu.edu.

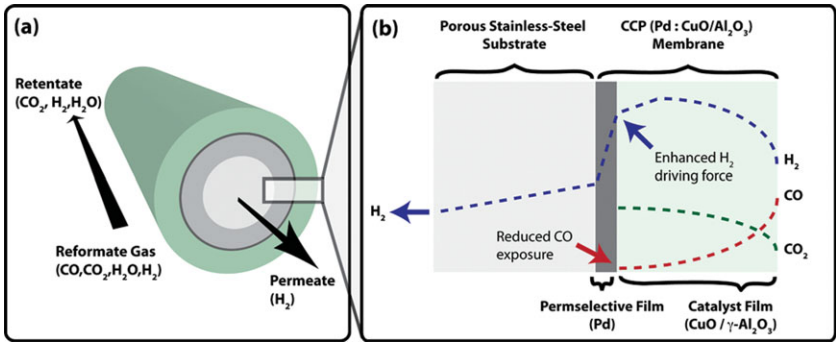

Figure 1. Schematic of the CCP membrane design, coupling a water–gas-shift catalytic film with dense palladium-permselective film for enhanced hydrogen removal from reformate mixtures.

[Color figure can be viewed in the online issue, which is available at wileyonlinelibrary.com.]

a reactive transport barrier that minimizes exposure of the underlying palladium film by catalytically eliminating one or more corrosive species while simultaneously increasing the local partial pressure of desired permeates. This technique was first demonstrated by Wilhite et al.[21] to prevent destructive corrosion of ultrathin (200 nm) palladium films by methanol reactant in a miniaturized membrane reformer. By applying a 500-μm catalytic layer (8:1 $LaNi_{0.95}Co_{0.05}O_3$/Al_2O_3), active for the irreversible partial oxidation of methanol, overtop the palladium film, corrosion was effectively prevented by the additional catalytic layer without contributing any additional resistance to hydrogen transport.[21]

Recently, one-dimensional (1-D) design analysis of the CCP membrane concept was presented for the case of (1) a general unimolecular reversible reaction and (2) the specific case of water–gas-shift catalyst film coupled with palladium-permselective film to minimize CO exposure from diesel reformate mixtures.[22] Inspection of the analytical solution to the reaction-diffusion model for the general case yielded general design criteria in terms of a modified catalyst Thiele modulus

$$\Phi\lambda = \left(\frac{r_0 \cdot t_c^2}{D_{\text{eff},i}}\right)^{1/2} \cdot \left(1 + \frac{1}{K_{\text{eq}} \cdot \alpha_{\text{C/A}}^{\text{cat}}}\right)^{1/2} = 7.6 \qquad (2)$$

which identify a catalyst film thickness sufficient to ensure 99.9% of the maximum possible reduction in corrosive species concentration by catalytic reaction, where r_0 is the rate of reaction consuming the corrosive species evaluated at bulk fluid inlet condition, $D_{\text{eff},i}$ is the effective diffusivity of the corrosive reactant in the catalyst film, $\alpha_{\text{C/A}}^{\text{cat}}$ is the relative permselectivity of reactant to reaction product, K_{eq} is the equilibrium coefficient for reaction, and t_c is the thickness of the catalyst film. This analysis also identified a second design parameter representing the extent of mass-transfer resistance imparted by addition of the catalytic layer

$$\zeta = \left(\frac{P_{H_2}^{\text{Pd}} \cdot p_{H_{2,\text{in}}}^{\text{F}}{}^{1/2}}{t_{\text{Pd}}}\right) \cdot \left(\frac{\text{RT}t_c}{D_{H_2,\text{eff}}}\right) \qquad (3)$$

and demonstrated that for the case of $\zeta \ll 1$ that addition of the catalyst layer would have no negative effect on permeation rates, that is, the full advantage of the CCP strategy may be achieved. Model analysis of a CCP architecture coupling reversible water–gas-shift reaction with a permselective palladium film for hydrogen recovery from diesel reformate predicted up to an 80% reduction in CO partial pressure at the catalyst–palladium interface relative to the bulk fluid CO partial pressure. Equivalent increases in hydrogen partial pressure at the palladium surface corresponded to a predicted enhancement of hydrogen permeation rates of ~5%, when neglecting any inhibitory effects of CO upon the palladium permeability. In light of the negative impact of CO upon palladium permeability, further enhancement of hydrogen permeation rates via reduced CO exposure may be expected using the CCP membrane design.

This manuscript details an experimental demonstration of enhanced hydrogen permeation in a dense palladium film by appropriate coupling with a water–gas-shift catalytic film using a CCP membrane architecture. Analysis of the resulting Cu(II)O/Al_2O_3:Pd composite membrane demonstrates the value of this design approach for improving hydrogen permeation rates, which is expected to translate into significant reduction in the capital costs associated with high-purity hydrogen production.[23,24]

Experimental

Substrate and palladium membrane preparation

Porous stainless-steel (PSS) tubes (Mott) with 0.5 μm grade [outside diameter (OD): 0.5 in., porous length: 2 in.] were used as supports for palladium thin-film deposition via electroless plating. The PSS supports were first cleaned in an ultrasonic bath of alkaline solution (sodium hydroxide, sodium carbonate, sodium phosphate, and organic detergent) at 333 K for 1 h to remove dirt and grease. The PSS tubes were thoroughly rinsed with deionized (DI) water, isopropanol, followed by oxidation at 673 K for 4 h using a heating and cooling rate of 3 K min^{-1}. The oxidation step is intended to grow a native surface oxide on the cleaned PSS tube surface for improving the stability of the palladium thin film by reducing intermetallic diffusion between the PSS and palladium.[25] Prior to electroless plating, the outer surface was activated with palladium nuclei by alternately immersing the tube in acidic $SnCl_2$ (200 mg $SnCl_2$ + 10 mL HCl + 100 mL H_2O) and $PdCl_2$ (30 mg $PdCl_2$ + 10 mL HCl + 100 mL H_2O) solutions until a uniform dark brown outer surface was observed. The activated PSS tube was then immersed vertically for 5 h at ambient temperature in a plating solution consisting of 28.2 mM PdCl (Sigma–Aldrich), 107 mM ethylenediaminetetraacetic acid disodium (Sigma–Aldrich), 4.05 M ammonium hydroxide (Fisher Scientific), 10 mM hydrazine (Sigma–Aldrich), and DI water. This plating procedure was repeated with fresh plating solution until a leak-free, dense

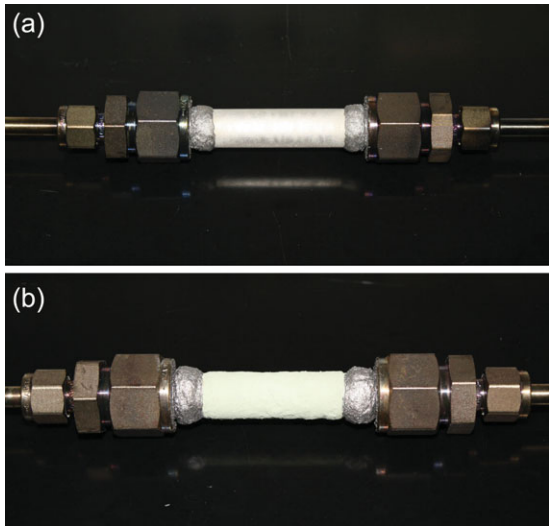

Figure 2. Membranes used in this work. (a) Palladium-plated PSS tube and (b) CCP membrane tube (catalyst layer + palladium film + PSS tube).

[Color figure can be viewed in the online issue, which is available at wileyonlinelibrary.com.]

film was achieved, as confirmed by helium permeation tests performed at ambient temperature after each plating. The resulting palladium membrane was estimated at 27 μm, as calculated by weight. Either end of the palladium-plated porous stainless-steel tube was then connected to a length of $^1/_2$-in. steel tubing using standard Swagelok fitting compression-sealed prior to catalyst coating (Figure 2a). High-temperature ceramic-metallic pastes (Pyro-Putty, Aremco Products) were applied to the two welds joining the porous and nonporous portions of the substrate, to compensate for pinholes and other defects observed in the welds.

Catalysts coating on palladium membranes

Crushed copper(II) oxide (13%) on alumina (3-mm sphere, Sigma–Aldrich) was uniformly washcoated over the palladium-permselective film to introduce the water–gas-shift reaction in proximity to the palladium surface. A target thickness of 500 μm was selected, assuming reaction rates predicted by the model of Mizsey et al.[26] Three grams of catalyst was placed in a mixture of 0.3 mL of 20% colloidal alumina (Alfa Aesar) and 21 mL of DI water and milled for 20 min in a ball mill (SPEX CertiPrep). Approximately 1 mL of resulting solution was applied to the horizontal membrane under steady rotation (40 rpm) and allowed to dry in ambient air for ~30 min. This procedure was repeated until a catalyst layer of ~500-μm thickness was achieved, as determined by measuring an increase in the outer diameter of the tube via a digital vernier caliper. The catalyst coating was then cured at 723 K for 4 h in the furnace under air environment with heating and cooling rates of 3 K min^{-1}. The resulting CCP membrane (Figure 2b) was then packed inside a $1^1/_2$-in. OD stainless-steel tube assembled with inlet and outlet ports to complete the membrane assembly (Figure 3, inset).

Water–gas-shift reaction coupled with palladium membranes

The schematic of the experimental apparatus used for all membrane analysis is shown in Figure 3. The membrane assembly was placed in a tube furnace (HST 12/200, Carbolite) and heated to 623 K at a heating rate of 3 K min^{-1}. During heating, nitrogen was supplied through the bore of the PSS tube (sweep) and 5%He/Ar was supplied into the annulus (feed) of the membrane assembly (Figure 3, inset). Once the furnace temperature reached 623 K, 15 mol % hydrogen was blended into the feed gas stream and permeate gas composition was analyzed by a mass spectrometer (RGA 100, Stanford Research Systems). After measuring hydrogen permeation through the catalytic-permselective membrane under ideal (hydrogen and inert gas) feed conditions, the surface of the catalyst layer was exposed to a gas mixture of 5% CO, 1.5% CO_2, 15% H_2, and 7.5% H_2O, representative of the composition expected from a diesel reformate mixture. Steam was supplied to the dry gas mixture using a gas bubbler maintained at constant temperature of 314 K via heating tape and digital controller (Omega) control for a target water vapor mole percent of 7.5%, as determined via Antoine equation.[27] Combined water–gas-shift reaction and hydrogen purification in the CCP membrane were investigated at 623, 673, 723, and 773 K at atmospheric pressure in both feed and sweep sides. The gas composition of the retentate in the hydrogen permeation system was analyzed by gas chromatography (GC, Agilent Technologies), and the permeate stream was analyzed by mass spectrometry. Feed stream makeup gas (5% He/Ar) provided an internal standard (helium) for determining outlet total molar flow rate via GC analysis. The CO conversion was determined from Eq. 3 as follows

$$X_{CO} = \frac{\dot{N}^F_{CO,out} + \dot{N}^F_{CO_2,out} + \dot{N}^F_{CH_4,out}}{\dot{N}^F_{CO,in}}. \quad (3)$$

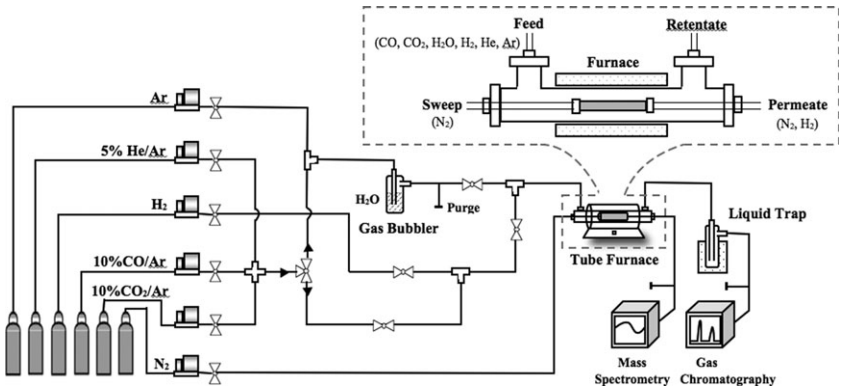

Figure 3. Schematic of experimental apparatus for gas separation experiments.

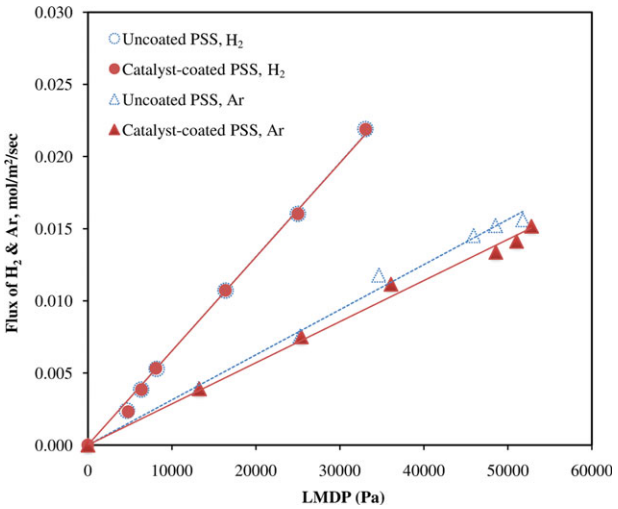

Figure 4. Hydrogen and argon flux through the uncoated and catalyst-coated PSS tubes as a function of LMDP.

[Color figure can be viewed in the online issue, which is available at wileyonlinelibrary.com.]

Analysis of gas permeation data was performed using approximately defined log-mean driving forces to account for the counter-current flow mode used in all experiments. For preliminary gas permeation tests of untreated and catalyst-coated porous stainless-steel substrates (in the absence of a dense palladium film), a first-order relationship between gas permeation and partial pressure is assessed, that is

$$F_i^{\mathrm{PSS,cPSS}} = P_i^{\mathrm{PSS,cPSS}}(\mathrm{LMDP_i}) \tag{4a}$$

where

$$\mathrm{LMDP_i} = \frac{(p_{i,\mathrm{in}}^{\mathrm{F}} - p_{i,\mathrm{out}}^{\mathrm{S}}) - (p_{i,\mathrm{out}}^{\mathrm{F}} - p_{i,\mathrm{in}}^{\mathrm{S}})}{\ln\left[\frac{(p_{i,\mathrm{in}}^{\mathrm{F}} - p_{i,\mathrm{out}}^{\mathrm{S}})}{(p_{i,\mathrm{out}}^{\mathrm{F}} - p_{i,\mathrm{in}}^{\mathrm{S}})}\right]} \tag{4b}$$

In the presence of a dense palladium film, hydrogen transport is assumed to follow a half-order dependence upon partial pressure in accordance with Sieverts' law governing hydrogen permeation through palladium.[8] Driving force is also defined to account for additional hydrogen partial pressures generated within the membrane by water–gas-shift reaction. The resulting definition for half-order log-mean driving force ($\mathrm{LMDP_{H2}^{1/2}}$) allows side-by-side comparison of CCP membrane performance under both reactive and nonreactive conditions

$$F_{\mathrm{H_2}} = P_{\mathrm{H_2}}^{\mathrm{Pd}}(\mathrm{LMDP_{H_2}^{1/2}}) \tag{5a}$$

where

$$\mathrm{LMDP_{H_2}^{1/2}} = \frac{(p_{\mathrm{H_2,in}}^{\mathrm{F}\ 1/2} + p_{\mathrm{CO,in}}^{\mathrm{F}\ 1/2} - p_{\mathrm{H_2,out}}^{\mathrm{S}\ 1/2}) - (p_{i,\mathrm{out}}^{\mathrm{F}\ 1/2} - p_{i,\mathrm{in}}^{\mathrm{S}\ 1/2})}{\ln\left[\frac{(p_{i,\mathrm{in}}^{\mathrm{F}\ 1/2} + p_{\mathrm{CO,in}}^{\mathrm{F}\ 1/2} - p_{i,\mathrm{out}}^{\mathrm{S}\ 1/2})}{(p_{i,\mathrm{out}}^{\mathrm{F}\ 1/2} - p_{i,\mathrm{in}}^{\mathrm{S}\ 1/2})}\right]} \tag{5b}$$

Results and Discussion

Initial characterization of substrate and catalyst layer permeances

Hydrogen and argon permeance of uncoated and catalyst-coated PSS tubes (in absence of palladium) were determined to isolate the influence of substrate (PSS tube) and catalyst layer upon gas permeation. The uncoated PSS tube (cleaned as per "Substrate and palladium membrane preparation" section) and the catalyst-coated PSS tube (washcoated as per "Catalysts coating on palladium membranes" section) were separately prepared and analyzed using a hydrogen–argon mixture as the feed gas and pure nitrogen as the sweep gas at a total flow rate of 96 mL $\mathrm{min^{-1}}$ each. Hydrogen and argon flux across the untreated and catalyst-coated substrates are presented as a function of log-mean difference of partial pressure (LMDP) in Figure 4. Permeances for hydrogen and argon ($P_{\mathrm{H_2}}$,P_{Ar}) are obtained by linear regression of the experimental data for both cases. The permeance of the catalyst film can then be estimated assuming a resistance-in series model across the catalyst-coated PSS substrate

$$\frac{1}{P_i^{\mathrm{c}}} = \frac{1}{P_i^{\mathrm{PSS}}} - \frac{1}{P_i^{\mathrm{c+PSS}}} \tag{6}$$

Resulting gas permeances measured for uncoated PSS substrate, catalyst-coated PSS substrate, and estimates for the catalyst layer are presented in Table 1. Accounting for propagation of error from measured to calculated permeances, the argon permeation data are sufficient to suggest a permeance for the catalyst film between 2.6 and 3.8 $\times$ 10^{-6} mol $\mathrm{m^{-2}\ s^{-1}\ Pa^{-1}}$, corresponding to an expected hydrogen permeance of 8.2–12 $\times$ 10^{-6} mol $\mathrm{m^{-2}\ s^{-1}\ Pa^{-1}}$ assuming transport is dominated by Knudsen diffusion.

Analysis of CCP membranes

Figure 5 illustrates hydrogen flux as a function of the square-root log-mean difference of driving force ($\mathrm{LMDP_{H2}^{1/2}}$) at 623, 673, 723, and 773 K. The first data point (hollow symbol) was obtained using 15 mol % hydrogen, balance argon, to ascertain membrane performance in the absence of reformate species (CO, $\mathrm{CO_2}$) or water–gas-shift reaction. The remaining experimental data points were obtained by introducing carbon monoxide, carbon dioxide, and steam (5% CO, 1.5% $\mathrm{CO_2}$, 7.5% $\mathrm{H_2O}$, 15% $\mathrm{H_2}$, and balance Ar) to observe CCP performance under water–gas-shift reaction at increasing feed gas flow rate.

Hydrogen permeation experiments were carried out using the catalyst-treated CCP membrane in the absence of water–

Table 1. Permeance of Hydrogen and Argon Through Uncoated PSS Tube (PSS), Catalyst-Coated PSS Tube (Cat. + PSS), and Only Catalyst Layer (Cat.) (Unit: mol $\mathrm{m^{-2}\ s^{-1}Pa^{-1}}$)

	PSS	Cat. + PSS	Cat.
$\mathrm{H_2}$	$6.52 \times 10^{-7} \pm 4.5 \times 10^{-9}$	$6.51 \times 10^{-7} \pm 2.0 \times 10^{-9}$	$4.24 \times 10^{-4} \pm 2.1 \times 10^{-5}$
Ar	$3.13 \times 10^{-7} \pm 3.9 \times 10^{-9}$	$2.85 \times 10^{-7} \pm 3.7 \times 10^{-9}$	$3.19 \times 10^{-6} \pm 6.1 \times 10^{-7}$

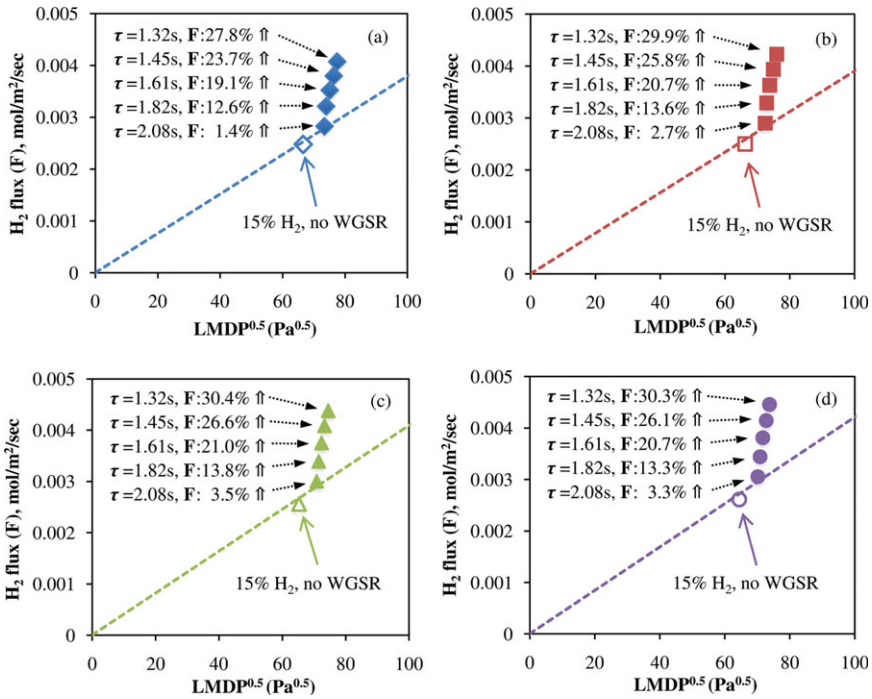

Figure 5. Hydrogen flux through the CCP membrane design at (a) 623, (b) 673, (c) 723, and 773 K.

[Color figure can be viewed in the online issue, which is available at wileyonlinelibrary.com.]

gas-shift contributions to characterize the palladium film after application of the catalyst washcoating. This enables a self-consistent analysis of the CCP membrane used, as permeances obtained in the presence of water–gas-shift contributions may be directly compared to the permeance of the identical palladium film. The first two data points obtained at each temperature are fit to a linear model (solid line, Figure 5) to obtain the permeance of the CCP in the absence of significant water–gas-shift contributions. Approximated first-order hydrogen permeances are summarized in Table 2, alongside the observed half-order hydrogen permeability obtained using the first two data points. Observed hydrogen permeances of the palladium film are an order-of-magnitude below the argon permeance estimated for the catalyst film (Table 1), indicating that the catalyst layer does not significantly contribute mass-transfer resistance to net hydrogen permeation. The dimensionless design group, ζ proposed by Wilhite[22] is $\sim 6.4 \times 10^{-2}$, which confirms that the catalyst layer in the CCP design has negligible effect on permeation rate. However, comparison of observed hydrogen permeance for the palladium film (Table 2) with values reported for the porous stainless-steel substrate (Table 1) indicate only a 3:1 ratio, suggesting that the PSS substrate does contribute noticeable mass-transfer resistance to net hydrogen permeation

Table 2. Observed Hydrogen Permeance and Permeability Through the Palladium Membrane in the CCP Membrane Design

	Permeance, mol m^{-2} $s^{-1}Pa^{-1}$	Permeability, mol m^{-1} s^{-1} $Pa^{-0.5}$
350°C	2.70×10^{-7}	1.00×10^{-9}
400°C	2.75×10^{-7}	1.02×10^{-9}
450°C	2.85×10^{-7}	1.06×10^{-9}
500°C	2.95×10^{-7}	1.09×10^{-9}
		$E_A = 2.3$ kJ mol^{-1}

across the CCP membrane, which results in a reduction in observed H_2 permeability as compared to values reported in the absence of substrate mass-transfer resistances.[8,9] Arrhenius analysis of palladium hydrogen permeability reported in Table 2 yields an observed activation energy of ~2.3 kJ mol^{-1}, confirming this observation. It should be noted that the presently reported values for observed H_2 permeability and activation energies are comparable to values previously obtained by Kim et al.[28,29] for electroless-deposited Pd films operating in the presence of substrate mass-transfer resistances.

At long residence times, hydrogen permeance in the presence of water–gas-shift reaction was comparable to that observed under ideal, or nonreacting (H_2-inert), environment. This can be attributed to the expectation that at high Damköhler number for reaction, the majority of the membrane is operating at equilibrium conditions, that is, negligible rate of reaction within the catalytic region of the composite membrane. As residence time is reduced, the percentage of the membrane operating under reaction-separation conditions is increased, thus, increasing the percentage of the system experiencing enhancement in permeation rates owing to water–gas-shift reaction within the membrane. This is reflected in ~30% increase in hydrogen flux with decreasing residence time observed at each temperature of study (Figure 5). Figure 6 compares observed CCP membrane permeances and corresponding CO conversions and H_2 recovery (%) as a function of residence time for each temperature. Results indicate that increases in membrane permeance of up to 30% coincide with a 30–42% increase in CO conversion corresponding to only a ~10% increase in total hydrogen available for permeation. Figure 6 also suggests an optimal residence time for maximizing water–gas-shift conversion in the CCP membrane. As residence time increases from zero, CO conversion initially increases toward a maximum value consistently greater than the corresponding equilibrium

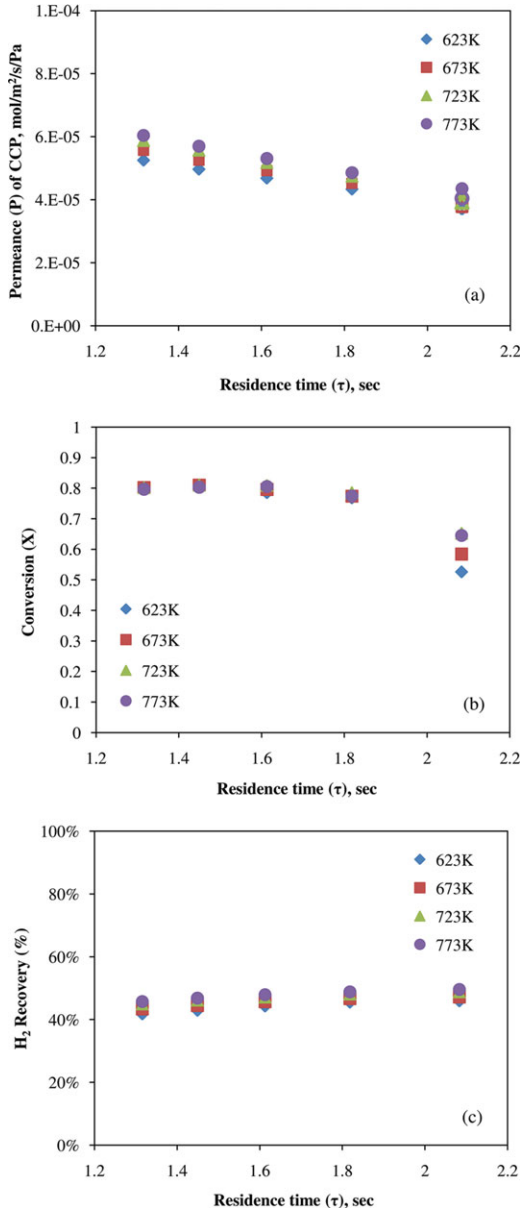

Figure 6. (a) Hydrogen permeance, (b) CO conversion, and (c) H_2 recovery (%) of CCP membranes as a function of residence time (τ) at 623, 673, 723, and 773 K.

[Color figure can be viewed in the online issue, which is available at wileyonlinelibrary.com.]

conversion, before reducing with further increases in residence time. This latter trend in conversion with residence time can be understood in terms of the enhancing effect of hydrogen permeation upon reaction conversion. As residence time increases, the driving force for hydrogen removal decreases owing to equilibration between the feed and sweep volumes; this reduced hydrogen removal rate reduces any enhancement of catalyst activity owing to hydrogen removal, in turn decreasing overall conversion.

Table 3 presents estimations for the kinetics- and shape-normalized[27] Thiele moduli corresponding to the experiments conducted using the estimated transport properties of the catalyst film and the rate expression presented by Mizsey[26] for the water–gas-shift reaction. Analysis confirms that

Table 3. Estimated Values for Shape- and Kinetics-Normalized Thiele Moduli for Catalyst Layer ($\Phi\lambda$) and Ratio of Palladium-to-Catalyst Hydrogen Permeance (ζ)

Temperature (K)	623	673	723	773
R_o (mol m^{-3} s^{-1})	15.6	31.4	56.7	93.2
C_o (mol m^{-3})	0.88	0.81	0.76	0.71
K	21	11.9	7.26	4.72
$D_{CO,N}$ (m^2 s^{-1})	6.9×10^{-6}	7.1×10^{-6}	7.4×10^{-6}	7.6×10^{-6}
$D_{H_2,K}$ (m^2 s^{-1})	2.4×10^{-5}	2.5×10^{-5}	2.6×10^{-5}	2.7×10^{-5}
$\Phi\lambda$	2.4	3.6	5.1	7.1
ζ	6.5×10^{-2}	6.4×10^{-2}	6.4×10^{-2}	6.4×10^{-2}

all experiments were performed in the presence of significant mass-transfer resistance to reactant diffusion within the catalyst film ($\Phi\lambda > 2$) with data obtained at 773 K corresponding to the criteria for maximum enhancement in permeation and corrosion reduction ($\Phi\lambda \sim 7.6$) identified by Wilhite.[22] Likewise, all experimental results are shown to be obtained under conditions wherein the catalyst permeance is significantly greater than the underlying palladium permeance ($\zeta \ll 1$, from Wilhite[22]), such that the benefits of the CCP strategy are observed without any reduction in hydrogen flux imparted by the catalyst layer. Thus, the present experimental work confirms the enhancement of hydrogen permeation through palladium thin films using the CCP membrane design for the present case of an unalloyed Pd film and a reformate mixture containing 4.5% CO at a steam-to-carbon

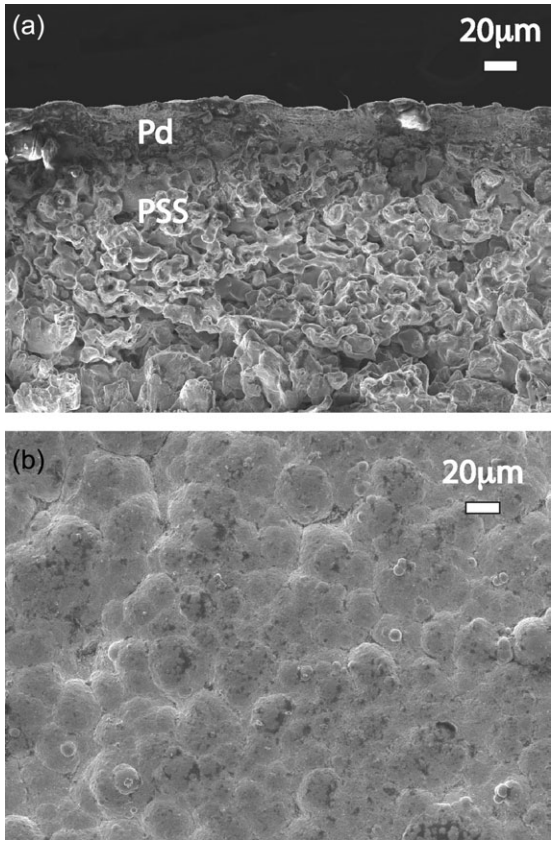

Figure 7. SEM images of (a) the cross-section and (b) surface of the palladium membrane plated over the PSS tube after completion of permeation experiments in the presence of water–gas-shift reaction (catalytic layer was removed from the palladium film).

ratio of 1.15:1. These conditions have been shown to correspond to significant inhibition of the Pd film by CO exposure;[30] ongoing efforts are aimed at studying the extent of membrane enhancement using the CCP membrane as a function of membrane resistance to CO by alloying of the Pd film or increasing the steam-to-carbon ratio, as well as exploring the performance of the CCP membrane design using permselective films of comparable permeance to the catalyst layer (i.e., $\zeta \sim 1$).

Throughout all tests, hydrogen permselectivity over argon remained over 10,000:1 corresponding to the lower level of carbon monoxide, carbon dioxide, or Argon detection limits of the permeate gas analysis. Maintenance of high selectivities even under reaction conditions confirms that palladium film stability was not compromised by coupling with water–gas-shift catalyst in the CCP membrane design. Scanning electron microscopy (SEM) images of the cross-section and surface of the palladium membrane upon completion of all experiments and subsequent removal of the catalyst film are presented in Figure 7. These images indicate that the dense $\sim$30-μm thick palladium film retained strong adhesion to the porous stainless-steel and did not develop defects (cracks, pinholes) even after $\sim$10 h of exposure to water gas shift reaction while in direct contact with the Cu(II)O–Al_2O_3 catalyst.

Interdiffusion of Cu from the catalyst washcoating to the palladium film may be expected to result in loss of palladium stability over long operating times (>100 h). This challenge to the CCP design may be met through introduction of an inert, porous oxide diffusion-barrier film between the palladium and catalyst layers; this strategy has already been demonstrated as a successful means of addressing long-term durability challenges associated with porous-metal supported palladium films.[8,9] For this reason, and in light of the present demonstration of the value of the CCP design for enhancing palladium permeance, future research is aimed at designing three-layer composite membrane designs.

Conclusions

The present experimental work confirms the enhancement of hydrogen permeation through dense palladium films via integration with water–gas-shift reaction in a CCP membrane, as previously predicted by 1-D analyses. Specifically, coupling of a 500-μm Cu(II)O/Al_2O_3 catalyst film with a 27-μm dense palladium film resulted in up to a 30% increase in hydrogen permeance for the case of hydrogen extraction from a simulated diesel reformate mixture (5% CO, 7.5% H_2O, 15% H_2, and 1.5% CO_2). Maintenance of hydrogen selectivities in excess of 10,000:1 during all experiments and SEM analysis of the palladium film upon completion of experiments confirm that film stability was not adversely affected by coupling with water–gas-shift catalyst. This design approach, thus, represents a cost-effective means of significantly enhancing the effectiveness of palladium membranes for hydrogen purification.

Acknowledgments

This work was supported by the National Science Foundation under award #0730820, (CBET Division, CBS Program). Additional financial support was provided by an NSF CAREER Award #078016 (CBET Division, CRE Program) and the Artie McFerrin Department of Chemical Engineering at Texas A&M University. The authors gratefully acknowledge Randy Marek of the chemical engineering department and Rodney Inmon of the aerospace engineering department at Texas A&M University for their technical assistance.

Notation

Symbols

Φ = shape- and kinetics-normalized Thiele modulus for cylindrical coordinate and second-order reaction
ζ = ratio of initial rates of hydrogen permeation through palladium and catalytic layers
τ = residence time, s

Letters

$D_{\mathrm{eff},i}$ = effective diffusivity of species i in catalyst, $m^2\ s^{-1}$
$D_{\mathrm{eff,K}}$ = Knudsen diffusivity of species i, $m^2\ s^{-1}$
F_i = molar flux of species i, mol $m^{-2}\ s^{-1}$
K_{eq} = equilibrium coefficient for water–gas-shift reaction
N_i = molar flow rate of species i, mol s^{-1}
p_i = partial pressure of species i, Pa
P_i = permeance of species i, mol $m^{-2}\ s^{-1}\ Pa^{-n}$
r_o = initial rate of water–gas-shfit reaction, mol $m^{-3}\ s^{-1}$
t = thickness of catalyst or palladium film, m
X_{CO} = conversion of carbon monoxide

Subscripts

Ar = argon
CH_4 = methane
c = catalyst film
CO = carbon monoxide
CO_2 = carbon dioxide
H_2 = hydrogen
H_2O = steam
Pd = palladium film

Superscripts

c = catalyst film
F = feed
Pd = palladium film
PSS = porous stainless-steel substrate
S = sweep

Literature Cited

1. Rifkin J. *The Hydrogen Economy*. New York: Tarcher/Putnam, 2002.
2. Gupta RB. *Hydrogen Fuel: Production, Transport, and Storage*. New York: CRC Press, 2009.
3. Newsome DS. The water gas shift reaction. *Catal Rev Sci Eng*. 1980;21:275–318.
4. Vielstich W, Lamm A, Gasteiger HA. *Handbook of Fuel Cells: Fundamentals, Technology, Applications*. New York: Wiley, 2003.
5. De Bruijn FA. The current status of fuel cell technology for mobile and stationary applications. *Green Chem*. 2005;7:132–150.
6. Kirubakaran A, Jain S, Nema RK. A review on fuel cell technology and power electronics interface. *Renew Sust Energy Rev*. 2009; 13:2430–2440.
7. Zamel N, Li X. Transient analysis of carbon monoxide poisoning and oxygen bleeding in a PEM fuel cell anode catalyst layer. *Int J Hydrogen Energy*. 2008;33:1335–1344.
8. Paglieri SN, Way JD. Innovations in palladium membrane research. *Sep Purif Methods*. 2002;31:1–169.
9. Ma YH, Akis BC, Ayturk ME, Guazzone F, Engwall EE, Mardilovich IP. Characterization of intermetallic diffusion barrier and alloy formation for Pd/Cu and Pd/Ag porous stainless steel composite membranes. *Ind Eng Chem Res*. 2004;43:2936–2945.
10. Sakamoto F, Kinari Y, Chen FL, Sakamoto Y. Hydrogen permeation through palladium alloy membranes in mixture gases of 10% nitrogen and ammonia in the hydrogen. *Int J Hydrogen Energy*. 1997; 22:369–375.
11. Sakamoto Y, Chen FL, Kinari Y, Sakamoto F. Effect of carbon monoxide on hydrogen permeation in some palladium-based alloy membranes. *Int J Hydrogen Energy*. 1996;210:1017–1024.
12. Amandusson H, Ekedhl L-G, Dannetun H. The effect of CO and O_2 on hydrogen permeation through a palladium membrane. *Appl Surf Sci*. 2000;153:259–267.

13. Catalano J, Baschetti MG, Sarti GC. Hydrogen permeation in palladium-based membranes in the presence of carbon monoxide. *J Membr Sci*. 2010;362:221–233.
14. Ali JK, Newson EJ, Rippin DWT. Deactivation and regeneration of Pd–Ag membranes for dehydrogenation reactions. *J Membr Sci*. 1994;89:171–184.
15. Gravil PA, Toulhoat H. Hydrogen, sulphur and chlorine coadsorption on Pd(111): a theoretical study of poisoning and promotion. *Surf Sci*. 1999;430:176–191.
16. Chen FL, Kinari Y, Sakamoto F, Nakayama Y, Sakamoto Y. Hydrogen permeation through palladium-based alloy membranes in mixtures of 10% methane and ethylene in the hydrogen. *Int J Hydrogen Energy*. 1996;21:555–561.
17. Jung SH, Kusakabe K, Morooka S, Kim S-D. Effects of co-existing hydrocarbons on hydrogen permeation through a palladium membrane. *J Membr Sci*. 2000;170:53–60.
18. O'Brien CP, Howard BH, Miller JB, Morreale BD, Gellman AJ. Inhibition of hydrogen transport through Pd and $Pd_{47}Cu_{53}$ membranes by H_2S at 350°C. *J Membr Sci*. 2010;349:380–384.
19. Opalka SM, Løvvik OM, Emerson SC, She Y, Vanderspurt TH. Electronic origins for sulfur interactions with palladium alloys for hydrogen-selective membranes. *J Membr Sci*. 2001;375:96–103.
20. Li A, Liang W, Hughes R. The effect of carbon monoxide and stream on the hydrogen permeability of a Pd/stainless steel membrane. *J Membr Sci*. 2000;165:135–141.
21. Wilhite BA, Weiss SE, Ying JY, Schmidt MA, Jensen KF. High-purity hydrogen generation in a microfabricated 23wt% Ag–Pd membrane device integrated with 8:1 $LaNi_{0.95}Co_{0.05}O_3/Al_2O_3$ catalyst. *Adv Mater*. 2006;18:1701–1704.
22. Wilhite BA. Composite catalytic-permselective membranes: a strategy for enhancing selectivity and permeation rates via reaction and diffusion. *Ind Eng Chem Res*. 2011;50:10185–10193.
23. Marcano JGS, Tsotsis TT. *Catalytic Membranes and Membrane Reactors*. Weinheim: Wiley-VCH, 2002.
24. Qi A, Peppley B, Karan K. Integrated fuel processors for fuel cell applications: a review. *Fuel Process Technol*. 2007;88:3–22.
25. Rothenberger KS, Cugini AV, Howard BH, Killmeyer RP, Ciocco MV, Morreale BD, Enick RM, Bustamante F, Mardilovich IP, Ma YH. High pressure hydrogen permeance of porous stainless steel coated with a thin palladium film via electroless plating. *J Membr Sci*. 2004;244:55–68.
26. Mizsey P, Newson E, Truong P, Hottinger P. The kinetics of methanol decomposition: a part of autothermal partial oxidation to produce hydrogen for fuel cell. *Appl Catal A*. 2001;213:233–237.
27. Green D, Perry R. *Perry's Chemical Engineer's Handbook*, 8th ed. New York: McGraw-Hill, 2008.
28. Kim D, Kellogg A, Livaich E, Wilhite BA. Towards an integrated ceramic micro-membrane network: electroless-plated palladium membranes in cordierite supports. *J Membr Sci*. 2009;340:109–116.
29. Kim D, Donohue D, Kuncharam B, Duval C, Wilhite BA. Toward an integrated ceramic micro-membrane network: effect of ethanol reformate on palladium membranes. *Ind Eng Chem Res*. 2010; 49:10254–10261.
30. Israni SH, Harold MP. Methanol steam reforming in Pd–Ag membrane reactors: effects of reaction system species on transmembrane hydrogen flux. *Ind Eng Chem Res*. 2010;49:10242–10250.

Manuscript received Mar. 20, 2012, and revision received Aug. 21, 2012.